Simulations of phase transitions in Rb_2ZnCl_4

H. M. Lu and J. R. Hardy

Department of Physics and Center for Electro-Optics, University of Nebraska–Lincoln, Lincoln, Nebraska 68588–0111

Abstract

Structural relaxations, molecular-dynamics simulations, and lattice-dynamics calculations were performed to study the phase transitions in Rb_2ZnCl_4, using intermolecular and intramolecular potentials generated from *ab initio* quantum-chemistry calculations for the whole molecular ion $ZnCl_4^{2-}$. Compared with an earlier treatment of the system by a polarizable-ion model, the present approach emphasizes the static effect of the electron covalency within the molecular ions that affects strongly both the intermolecular and intramolecular interactions. The calculations gave a close agreement with experiment on the static structures of the *Pnam* and the $Pna2_1$ phases and the transition temperature from the former to the latter. For the lower-temperature, monoclinic phase of Rb_2ZnCl_4, the detailed structure of which is unknown, our simulations predict a structure with $C1c1$ space-group symmetry, which doubles the $Pna2_1$ structure along both the b and c axes and thus has 48 formula units per unit cell. The lattice-dynamics calculations for the $Pna2_1$ structure clearly revealed the lattice instability responsible for the $Pna2_1$-monoclinic transition and provided a more convincing explanation of a previous Raman measurement. We have shown that the potential-energy surface in Rb_2ZnCl_4 pertinent to the phase transitions contains a double-well structure, very similar to that of K_2SeO_4, except that the double well is much deeper, causing the much more severe disordering in the *Pnam* structure of Rb_2ZnCl_4 observed experimentally.

Simulations of phase transitions in Rb_2ZnCl_4

H. M. Lu and J. R. Hardy

Department of Physics and Center for Electro-Optics, University of Nebraska–Lincoln, Lincoln,
Nebraska 68588–0111

Structural relaxations, molecular-dynamics simulations, and lattice-dynamics calculations were performed to study the phase transitions in Rb_2ZnCl_4, using intermolecular and intramolecular potentials generated from *ab initio* quantum-chemistry calculations for the whole molecular ion $ZnCl_4^{2-}$. Compared with an earlier treatment of the system by a polarizable-ion model, the present approach emphasizes the static effect of the electron covalency within the molecular ions that affects strongly both the intermolecular and intramolecular interactions. The calculations gave a close agreement with experiment on the static structures of the *Pnam* and the $Pna2_1$ phases and the transition temperature from the former to the latter. For the lower-temperature, monoclinic phase of Rb_2ZnCl_4, the detailed structure of which is unknown, our simulations predict a structure with $C1c1$ space-group symmetry, which doubles the $Pna2_1$ structure along both the b and c axes and thus has 48 formula units per unit cell. The lattice-dynamics calculations for the $Pna2_1$ structure clearly revealed the lattice instability responsible for the $Pna2_1$-monoclinic transition and provided a more convincing explanation of a previous Raman measurement. We have shown that the potential-energy surface in Rb_2ZnCl_4 pertinent to the phase transitions contains a double-well structure, very similar to that of K_2SeO_4, except that the double well is much deeper, causing the much more severe disordering in the *Pnam* structure of Rb_2ZnCl_4 observed experimentally.

I. INTRODUCTION

Rubidium tetrachlorozincate (Rb_2ZnCl_4) undergoes three successive phase transitions. Above 302 K, it takes the β-K_2SO_4 structure, like many other members in the family of the A_2BX_4 compounds. It is paraelectric and has four formula units in an orthorhombic cell (space group *Pnam*). At 303 K it transforms to an incommensurate structure with the incommensurate modulation vector $q=[(1-\delta)a^*]/3$, where a^* is the first reciprocal-lattice vector along the [100] direction and $\delta \ll 1$. As the temperature is lowered further, the parameter δ decreases monotonically and vanishes at 189 K when the system locks into a ferroelectric superstructure (space group $Pna2_1$), whose a axis is triple the size of that of the *Pnam* phase. When cooled further, Rb_2ZnCl_4 undergoes another transition at 74 K to a monoclinic lattice, the specific space group of which is still not quite clear. These phase transitions, especially the commensurate-incommensurate transition, have attracted extensive experimental as well as theoretical efforts.[1–5]

A simulational study of the *Pnam* paraelectric structure of Rb_2ZnCl_4 at the microscopic level was made by Edwardson *et al.*[3] using Gordon-Kim[6] interionic poten-

tials. The approach was based on the rigid-ion approximation and the assumption that the ions in the crystal have their full ionicity, i.e., Rb^{1+}, Zn^{2+}, and Cl^-. Two major discrepancies exist between the resultant theoretical structure and the experimental data: (1) the Zn—Cl bond was too long, a discrepancy which had to be removed by a rescaling of the Zn—Cl short-range potential, and (2) the molecular ions $ZnCl_4^{2-}$ were rotated fairly substantially about the c axis away from their experimental orientations. It was pointed out in Ref. 3 that these could be due to the fact that the rigid-ion approximation is breaking down for the system, i.e., the polarization of the ions should be taken into account. This was done in Ref. 4, where the ions were allowed to polarize in nonlinear response to the forces. The agreement between theory and experiment has been greatly improved. In particular, the Zn-Cl bond lengths are within 1–2% from the experimental values and the $ZnCl_4^{2-}$ ions assume essentially the correct orientations.

However, as pointed out in Refs. 3 and 4, there is another direction in which the answers to the large discrepancies between the experimental data and the basic theoretical model in Ref. 3 may be sought; that is, by questioning the assumption that the ions in Rb_2ZnCl_4

retain their full ionicity. In fact, it has been found that a $+1$ charge for Zn and -0.75 charge for Cl, when placed at the experimentally determined positions of the atoms in Rb_2ZnCl_4, will best reproduce the electromagnetic field gradients as measured by nuclear magnetic resonance.[7] If there is indeed such a charge transfer within the $ZnCl_4^{2-}$ ion, indicating the importance of electron covalency in the system, then the large discrepancy between theory and experiment in Ref. 3 would not be so surprising. The intermolecular interactions will definitely be affected by the very different charges from the incomplete ionicity, which may explain the incorrect orientations of the $ZnCl_4^{2-}$ ions. Furthermore, the electron covalency within the $ZnCl_4^{2-}$ ion clearly renders the intramolecular interaction incapable of description by a Gordon-Kim model based on the assumption that the total charge density of a pair of interacting ions is a superposition of the charge densities of the individual ions. This could be the origin for the long Zn-Cl bond lengths.

Recently, we have developed a first-principles approach to the description of interionic interactions, specifically for ionic molecular crystals, where the covalent electron charge transfer within the molecular ions discussed above is important.[8] We have applied the method to K_2SeO_4, another member of the A_2BX_4 family, for which the basic model used in Ref. 3 would give similar discrepancies between theory and experiment as for Rb_2ZnCl_4 and the full ionicity assumption is more obviously incorrect since it would give the Se atoms unrealistically large ionicity of $6+$. Our method starts from performing *ab initio* quantum-chemistry calculations for the whole molecular ion, i.e., the SeO_4^{2-} tetrahedron. These calculations produce realistic electron chargedensity distribution that correctly takes into account the electron covalency within the molecular ion and therefore leads to a correct description of the intermolecular interactions. The resultant effective ionicities for the atoms are $+1.1504$ for Se and -0.7876 for O, respectively. As for the intramolecular interactions, we employ a harmonic expansion of the total energy of the molecular ion with the expansion coefficients also determined by the *ab initio* quantum-chemistry calculations. Using these intramolecular and intermolecular potentials, we have successfully reproduced the experimental structures, simulated the cell-tripling phase transition, and revealed the origin of the phase transition as the double-well structure on the potential-energy surface.[8]

In the present work, we apply this method to Rb_2ZnCl_4. We performed *ab initio* quantum-chemistry calculations for the molecular ion $ZnCl_4^{2-}$ and computed the intermolecular and intramolecular potentials from these calculations. The effective ionicities of the Zn and Cl atoms are 0.9508 and -0.7377, respectively, in close agreement with those found in Ref. 7 by fitting the experimental data. On the basis of the resultant *ab initio* potential-energy surfaces, we performed relaxations for the static structure of both the *Pnam* and the $Pna2_1$ phases of Rb_2ZnCl_4 and obtained close fits to the experimental data. Then the method of molecular dynamics (MD) was used to simulate directly the dynamical states of Rb_2ZnCl_4 at various temperatures. With a supercell

containing 672 atoms, we simulated the transition from the *Pnam* phase to the $Pna2_1$ phase and to the monoclinic phase at lower temperature with the theoretical transition temperatures, yielding a close agreement with the experimental values. Since no structural data have been given in the literature on the monoclinic phase, except for some conflicting suggestions about the space-group symmetry, our theoretical structure could be important in resolving the issue. Through lattice-dynamics calculations for the *Pnam* structure, we showed that the potential-energy surfaces pertinent to the phase transitions under consideration contain a double-well type of structure, very similar to that found in K_2SeO_4.[8] Our lattice-dynamics calculations for the $Pna2_1$ structure clearly show that the $Pna2_1$-monoclinic phase transition should be a modulation with the wave vector $q=(b^*+c^*)/2$. This is in accord with the suggestion by Wada *et al.* that the phase transition doubles the $Pna2_1$ unit cell.[9]

This paper is organized as follows: In Sec. II we outline the procedure for obtaining the intramolecular and intermolecular potentials from quantum-chemistry calculations. Section III gives the results of static relaxation for both the *Pnam* and the lower-temperature $Pna2_1$ structures. In Sec. IV, we describe molecular-dynamics calculations to simulate the phase transitions in Rb_2ZnCl_4. Section V considers qualitatively the lattice instability from the point of view of lattice dynamics and discusses the driving mechanism of the transition. Section VI concludes the paper.

II. CALCULATIONS OF THE *AB INITIO* INTERMOLECULAR AND INTRAMOLECULAR POTENTIALS

A full description of the procedure for obtaining interionic potentials from *ab initio* quantum-chemistry calculations has been given in Ref. 8, therefore here we only outline the steps. We first performed a quantum-chemistry structural optimization for the $ZnCl_4^{2-}$ ion, which searches for the atomic configuration that gives the lowest self-consistent Hartree-Fock energy. Such an optimization is necessary to provide an equilibrium structure for a harmonic expansion of the total energy of the molecular ion as a function of the bond lengths, bond angles, etc. The optimized $ZnCl_4^{2-}$ forms a perfect tetrahedron with the Zn-Cl bond length being 4.385 a.u., fairly close to the experimental average value of 4.239 a.u. in the *Pnam* phase.[10] This indicates that a harmonic expansion of the energy at the optimized structure should provide a reasonable description for the intramolecular interactions. *Ab initio* force constants for the optimized structure were then calculated to be used for this harmonic expansion.

Next we calculated the electron charge-density distribution for the $ZnCl_4^{2-}$ ion at the optimized structure. This charge-density distribution was then decomposed[8] into approximate charge densities for the individual Zn and Cl atoms. Using these charge densities and the free ion charge density for the Rb^+ ion,[11] we computed the

short-range pair potentials between these ions according to the Gordon-Kim electron-gas model.[6] For the long-range Coulomb forces, the ionicities on the ions were 1+ for Rb, 0.9598 for Zn, and −0.7377 for Cl, where the fractional charges were obtained from the computed charge density of ZnCl$_4{}^{2-}$ by a Mulliken population analysis.[12] The quantum-chemistry calculations were performed using the GAUSSIAN 86 program.[13] We used the standard STO-3G basis set for Zn and 6-31G basis set for Cl. The single first polarization functions were also added to the basis for both atoms.

As in the case for K$_2$SeO$_4$, our quantum-chemistry calculations were made for an isolated molecular ion and thus did not include a background crystal field. Such a background crystal field will definitely affect the electron charge density of ZnCl$_4{}^{2-}$, but these effects may well be unimportant for the following reason. By regarding the atoms as point charges with the values cited above, we calculated the electric fields at the atomic cites in the experimental *Pnam* structure. We found that, while the dominant fields are those on the chlorine atoms, over 90% of the contribution to these fields is from the other ions in the same ZnCl$_4{}^{2-}$ ion, rather than from the rest of the lattice. Therefore, our quantum-chemistry calculation for the whole molecular ZnCl$_4{}^{2-}$ ion has, in fact, included most of the crystal-field effects. Although the remaining crystal fields due to the rest of the lattice may affect, to some degree, the shapes of the tails of the electron charge distributions on the outskirts of the ZnCl$_4{}^{2-}$ ion, they are relatively unimportant in determining the electron charge distribution within, and close to, the molecular ion which is most crucial for the intramolecular and intermolecular interactions.

III. STATIC STRUCTURES FOR THE *Pnam* AND *Pna*2$_1$ PHASES

Once the intramolecular and intermolecular potentials were determined, we then performed static relaxations for the *Pnam* and *Pna*2$_1$ structures of Rb$_2$ZnCl$_4$. These relaxations give crystal structures that are at extremes of the theoretical potential-energy surface where the forces on the basis ions are zero. We constrained the relaxations to these two symmetries since this will allow us to concentrate on part of the phase space that is pertinent to the phase transitions under consideration. By comparing the atomic positions in the relaxed structures with their experimental counterparts, we then have a sensitive test
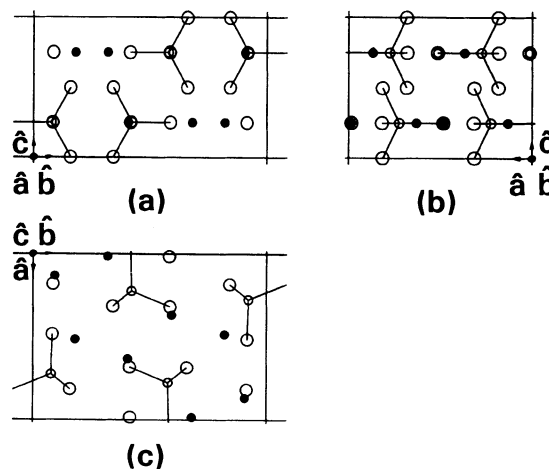

FIG. 1. Projections of the experimentally determined average structure Rb$_2$ZnCl$_4$ in the *Pnam* phase. Unit vectors indicate the directions of the lattice basis vectors. A unit vector pointing out of the page is represented by a circle. The Rb atoms are represented by solid circles, Zn atoms by small open circles, and Cl atoms by large open circles. Bonds (straight lines) connect each Zn and the nearest four Cl atoms.

of the validity of the intramolecular and intermolecular potentials.

First we consider the *Pnam* structure of Rb$_2$ZnCl$_4$. Figure 1 shows the projections of the experimental atomic positions parallel to each of the three orthorhombic axes [$a = 17.501$ a.u., $b = 24.047$ a.u., and $c = 13.757$ a.u. (Ref. 10)]. The prototypic parameters for the experimental structure[10] are given in Table I in parentheses. Our relaxation started from the experimental structure and used a Newton-Raphson algorithm. The Ewald summation technique was used for the calculation of the lattice energy and forces, etc., for the infinite lattice obtained by applying periodic boundary conditions.

Projections of the atomic positions in the relaxed structure are shown in Fig. 2 with the positional parameters given in Table I. The lattice constants for the relaxed structure are $a = 16.650$ a.u., $b = 23.614$ a.u., and $c = 13.416$ a.u., and they fall short of the experimental values by 4.9% for a, 1.8% for b, and 2.5% for c. This shortening has been a rather general feature for large unit-cell simulations using Gordon-Kim potentials and appeared similarly in our simulation for K$_2$SeO$_4$. Al-

TABLE I. Prototypic atomic positions for Rb$_2$ZnCl$_4$ in the relaxed *Pnam* structure. Experimental values (Ref. 10) are given in parentheses.

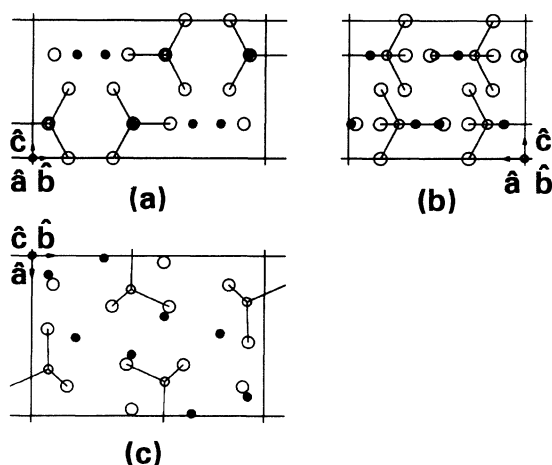| Prototype	x/a	y/b	z/c	Wyckoff site designation
Zn	0.2120 (0.2245)	0.4263 (0.4224)	$\frac{1}{4}$	4c
Rb(1)	0.1189 (0.1316)	0.0701 (0.0933)	$\frac{1}{4}$	4c
Rb(2)	0.9859 (0.9851)	0.6893 (0.6807)	$\frac{1}{4}$	4c
Cl(1)	0.3173 (0.3154)	0.3464 (0.3417)	−0.0017 (0.0012)	8d
Cl(2)	0.3190 (0.3183)	0.5909 (0.5858)	$\frac{1}{4}$	4c
Cl(3)	−0.0406 (−0.0159)	0.4319 (0.4170)	$\frac{1}{4}$	4c

FIG. 2. Projections of the theoretical structure obtained by static relaxation with *Pnam* constraint.

though these deviations are certainly not negligible in magnitude, they are, however, percentagewise comparable in all three dimensions. Moreover, the ratio b/c, a crucial parameter for the "latent symmetry" that drives the incommensurate phase transition in this system,[2,5] is 1.76, in good agreement with the value 1.75 for the experimental structure. This indicates, while the discrepancies in the absolute lengths of the axes are significant, the more or less uniformly contracted theoretical structure should still preserve those basic symmetries of the system relevant to the phase transitions under study.

The theoretical basis parameters are in close agreement with the experimental values as shown in Table I. The largest difference is 0.025 for x/a of Cl(3), which gives a displacement of about 0.5 bohr, well below the thermal fluctuations in the positions of the ions in the *Pnam* phase.[14] As we mentioned earlier, the Zn—Cl bond length in the theoretical structure obtained using the basic model in Ref. 3 was too long compared with the experimental value and the $ZnCl_4^{2-}$ ions have rotated about the c axis. None of these discrepancies appeared in the present relaxed structure: the average Zn—Cl bond length is 4.244 a.u., only 0.12% longer than the experimental value of 4.239 a.u.; the $ZnCl_4^{2-}$ ions shown in Fig. 2 essentially have the same orientations as those in the experimental structure Fig. 1. This indicates that the present method gives a good description for the potential-energy surface pertinent to the *Pnam* structure of Rb_2ZnCl_4, at least equally good as the polarizable ion model employed in Ref. 4.

Next we performed static relaxation for the ferroelectric $Pna2_1$ structure of Rb_2ZnCl_4 to examine further the potential-energy surface. Figure 3 shows projections of the experimental atomic positions measured at 100 K.[7] The lattice is orthorhombic $Pna2_1$ with $a = 51.977$ a.u., $b = 23.870$ a.u., and $c = 13.685$ a.u., and the experimental prototypic atomic positions are given in parentheses in Table II.[7] Comparing the structure in Fig. 3 and the *Pnam* structure in Fig. 1, we see that the unit cell in the $Pna2_1$ structure can be considered as formed by tripling the unit cell of the *Pnam* structures along the **a** axis and then slightly modulating the structures in each of the original *Pnam* cells. The modulation mainly consists of the rotation of the $ZnCl_4^{2-}$ ions about the a axis and the shifting of the Rb^+ ions in c direction. This tripling of the structure is a result of the lock-in from the incommensurate phase that exists between the *Pnam* and $Pna2_1$

TABLE II. Prototypic atomic positions for Rb_2ZnCl_4 relaxed within $Pna2_1$ constraints. Experimental values (Ref. 7) are given in parentheses.

Prototype	x/a	y/b	z/c	Wyckoff site designation
Zn(1)	0.0724 (0.0735)	0.4204 (0.4222)	0.2564 (0.2500)	4a
Zn(2)	0.7412 (0.7414)	0.4152 (0.4208)	0.2362 (0.2551)	4a
Zn(3)	0.4044 (0.4072)	0.4174 (0.4208)	0.2841 (0.2706)	4a
Rb(1)	0.2113 (0.2089)	0.4204 (0.4047)	0.2280 (0.2424)	4a
Rb(2)	0.0443 (0.0424)	0.0834 (0.0900)	0.2885 (0.2804)	4a
Rb(3)	0.3817 (0.3769)	0.0818 (0.0987)	0.2665 (0.2639)	4a
Rb(4)	0.1666 (0.1631)	0.8107 (0.8189)	0.2419 (0.2452)	4a
Rb(5)	0.3326 (0.3292)	0.6937 (0.6807)	0.2220 (0.2498)	4a
Rb(6)	0.5001 (0.4960)	0.8076 (0.8182)	0.2992 (0.2805)	4a
Cl(1)	0.6594 (0.6604)	0.4365 (0.4205)	0.3123 (0.2794)	4a
Cl(2)	0.3218 (0.3261)	0.4438 (0.4199)	0.3232 (0.2916)	4a
Cl(3)	−0.0080 (−0.0068)	0.4490 (0.4252)	0.1701 (0.2058)	4a
Cl(4)	0.1144 (0.1084)	0.5767 (0.5825)	0.3308 (0.3010)	4a
Cl(5)	0.7816 (0.7754)	0.5734 (0.5824)	0.1599 (0.1993)	4a
Cl(6)	0.4468 (0.4408)	0.5754 (0.5839)	0.3424 (0.3029)	4a
Cl(7)	0.1125 (0.1101)	0.3580 (0.3624)	−0.0025 (−0.0141)	4a
Cl(8)	0.7539 (0.7656)	0.2868 (0.3082)	0.0170 (0.0308)	4a
Cl(9)	0.4285 (0.4351)	0.3591 (0.3562)	0.0023 (−0.0001)	4a
Cl(10)	0.4334 (0.4384)	0.2901 (0.3168)	0.4851 (0.4954)	4a
Cl(11)	0.7808 (0.7750)	0.3614 (0.3654)	0.4999 (0.5245)	4a
Cl(12)	0.0814 (0.0950)	0.2970 (0.3127)	0.4849 (0.4812)	4a

phases.[7,15]

We performed a static relaxation with the $Pna2_1$ symmetry constraint starting from the experimental structure given in Fig. 3. The relaxed theoretical structure is shown in Fig. 4 and the positional parameters for structure are given in Table II. The lattice constants are $a = 50.088$ a.u., $b = 23.039$ a.u., and $c = 13.657$ a.u., again shorter than the experimental values (3.6% for a, 3.4% for b, and 0.2% for c, but no worse than for the $Pnam$ phase.

Comparing Fig. 4 with Fig. 3, we see that our relaxation gives a close fit to the experimental data. The largest discrepancy in the reduced basis positions is 0.039 for z/c of Cl(6), as shown in Table II, which would mean an actual displacement of 0.53 bohr if the experimental lattice constant c is used. Again, this is below the thermal fluctuation of these ions found in experiment.[7] Overall the basic modulation in the experimental structure is closely reproduced, although the amplitude of the modulation is slightly larger, as is to be expected from the comparison

of a static modulation with the experimental dynamical average at 100 K.[7]

Regarding the atoms as point charges and using the atomic positions in the theoretical static $Pna2_1$ structure, we calculated the dipole moment for the unit cell and found that the theoretical structure possesses a spontaneous polarization along the c axis as found by experiment.[16] Its magnitude is 0.418 μC/cm^2, a little larger than the value obtained by using the experimental atomic positions,[7] 0.265 μC/cm^2. This is consistent with the fact the amplitude of modulation in the theoretical structure is larger than that in the experimental structure, as pointed out above, since the polarization is purely the result of the modulation. Both of these values, however, are much larger than the experimental spontaneous polarization of 0.12 μC/cm^2 as measured at 153 K.[16] This is again due to the fact that the theoretical values above are for static structures and thermal effects have to be included when a direct comparison with experimental value is made. We therefore performed a molecular-dynamics simulation for
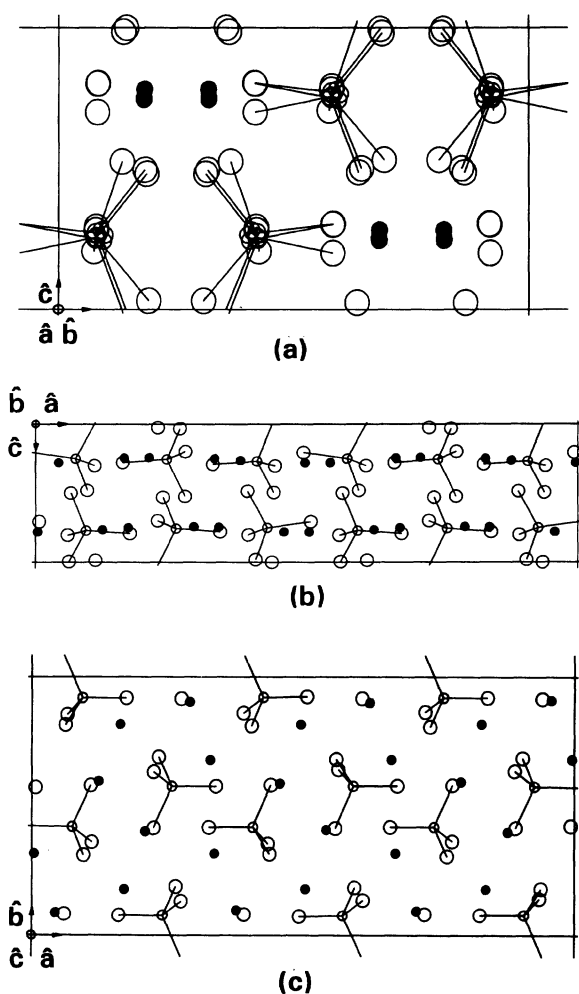

(a)

(b)

(c)

FIG. 3. Projections of the experimentally determined average structure of Rb$_2$ZnCl$_4$ in the $Pna2_1$ phase. Note that the a axis is approximately triple that in the $Pnam$ structure in Fig 1.
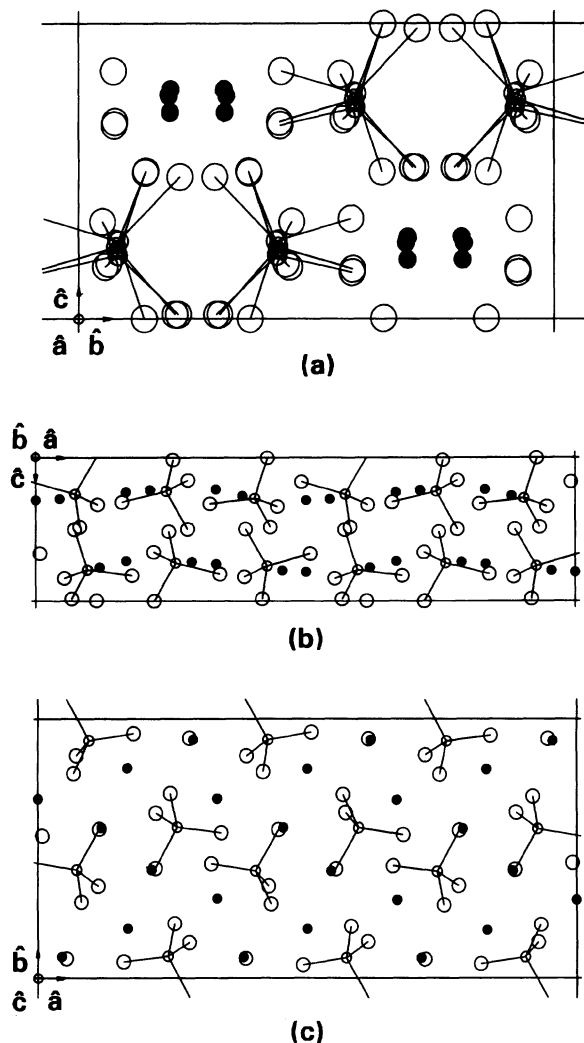

(a)

(b)

(c)

FIG. 4. Projections of the theoretical structure obtained by static relaxation with $Pna2_1$ constraint.

a $Pna2_1$ unit cell (84 atoms) at 150 K for a period of 20 ps. The obtained average polarization is 0.116 $\mu C/cm^2$, in good agreement with the experimental value.

IV. MOLECULAR-DYNAMICS SIMULATIONS

First, we simulated the dynamical state of the $Pnam$ structure of Rb_2ZnCl_4, since this would further test our *ab initio* potential-energy surface for the system. It has been shown[14] that this phase is highly disordered—each tetrachlorozincate group librates between two possible equivalent orientations and the $Pnam$ symmetry is only the result of a long-time average. In order to obtain such an average structure with a reasonable amount of computer time, we chose a relatively small supercell and a fairly high temperature to increase the speed of the librations of the tetrachlorozincate ions. The supercell was formed by first tripling the $Pnam$ unit cell along the a axis and then doubling it along the c axis. The sample was heated to 500 K and then the average structure over the period of 100 ps was calculated. Our MD simulation followed a constant-(zero-) pressure algorithm[17] and applied no restriction on the sample besides the periodic boundary condition, i.e., all of the atomic positions and all of the lattice vectors were allowed to vary during the simulation. The time increment between two successive steps was 0.005 ps, which was found to be sufficiently short.

Figure 5 shows the projections of the atomic positions on the ac plane in the obtained average structure. The ellipsoids centered at the average atomic positions indicate the amplitudes of the thermal motions of the atoms. The large sizes of these ellipsoids and the elongated shapes of those of the Cl atoms clearly show that the $ZnCl_4^{2-}$ tetrahedra undergo librations about the Zn atoms. In the perfect $Pnam$ structure, one of the Zn—Cl bonds for each $ZnCl_4^{2-}$ tetrahedron is parallel to the a axis, as can be seen in Fig. 1(b). The librations of the $ZnCl_4^{2-}$ tetrahedra cause these bonds to tilt up and down around the a axis. In Fig. 5 we see that these bonds are very close to
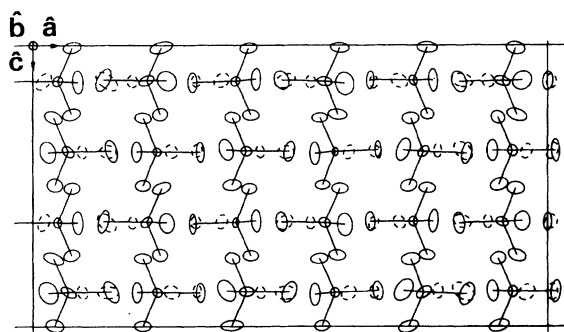

FIG. 5. Projections of the atomic positions along the b axis in the average structure at $T = 500$ K obtained from the MD simulation discussed in the text. The ellipsoids centered at the atomic positions (dashed-line circles for Rb atoms and solid-line circles for Zn and Cl atoms) indicate the amplitudes of the thermal motions of the atoms. Bonds connect the average positions of the Zn atom and those of the nearest four Cl atoms.

their ideal orientations and the structure is quite close to a perfect $Pnam$ structure. We found that the longer time we take to calculate the average, the more true this is. This clearly matches the disordering picture for the $Pnam$ phase proposed in Ref. 14.

A point worth mentioning is that, in a MD simulation of the $Pnam$ phase of the isomorph K_2SeO_4, the average time to obtain an almost perfect $Pnam$ structure was 2 ps, much shorter than that for the present system. This is consistent with the fact that, in K_2SeO_4, the disordering of the orientations of the molecular ions is much "milder," since it was only found via light-scattering experiments[18] that probe relatively fast motions of the atoms. But in Rb_2ZnCl_4, the disordering manifests itself even in x-ray measurements.[14] This shows that the librations of the molecular ions that cause the disordering of the $Pnam$ structure in K_2SeO_4 and in Rb_2ZnCl_4 involve significantly differnt time scales, although the driving mechanism for the disordering is basically the same, as will be shown in the next section.

Next we simulated the transition from the $Pnam$ structure to the lower temperature phases. We used a supercell containing 24 of the $Pnam$ unit cells of Rb_2ZnCl_4 with a total of 672 atoms. It was formed by first tripling the $Pnam$ unit cell along the a axis, allowing the experimentally observed cell-tripling transition to take place, and then doubling along the b axis and quadrupling along the c axis, allowing a possible doubling along these two directions as suggested by some experimental work.[9] The quadrupling along the c axis rather than just doubling is to make the three dimensions of the supercell comparable, since we believe this is important for the MD simulations to sample the right phase space pertinent to the transitions.

Starting from the $Pnam$ structure, we first heated the sample to abut 600 K and then quenched it down gradually by reducing the kinetic energy in steps. At each step the sample was allowed to equilibrate for 10 ps and the average temperature and average positions of the atoms were calculated. Although it is clear from the earlier MD simulation with 100 ps that 10 ps is far from enough for the relatively large supercell to average out the disordering of the molecular ions for the $Pnam$ phase, and increase of this average time is well beyond our computing resources since the present calculation already took approximately 20 days of CPU time on a Digital Equipment Corporation (DEC) Station 5000 (~40 h on a Cray Research Y-MP supercomputer). However, the simulation still closely reproduced the lower-temperature phase transitions, as we shall see.

From the simulation we obtained average structures at temperatures over the range 0–600 K, at roughly 20 K apart. Because of the relatively short average time at each temperature, all of the $ZnCl_4^{2-}$ ions appear in the disordered positions at high temperatures so that the original $3a \times 2b \times 4c$ periodicity within the supercell seem to have completely disappeared. However, by comparing the average structures, we found that, above 300 K, many of the $ZnCl_4^{2-}$ ions change from one disordered position to another, crossing their orientations in the perfect $Pnam$ structure. This indicates that the system at

these temperatures is still in the *Pnam* phase.

Experimentally, Rb$_2$ZnCl$_4$ transforms from the high-temperature *Pnam* phase first to an incommensurate phase and then locks into a supercell structure that triples the *Pnam* unit cell along the **a** axis. Because of the periodic boundary conditions applied to the supercell, the current MD simulation cannot describe the incommensurate state of the system. However, since the incommensurate wave vector is $q = [(1-\delta)a^*]/3$, representing an incommensurate period close to triple of the *Pnam* unit cell, the incommensurate and the subsequent lock-in transition should show as a "combined" transition in the simulation.

In order to monitor this *Pnam*-*Pna*2_1 transition, we calculated a quantity Q as a convenient order parameter. This is obtained as follows: first, we calculated the normalized displacements of the atoms in the theoretical *Pna*2_1 structure obtained in Sec. III from their ideal positions in the theoretical *Pnam* structures. These displacements form a $3N$-dimensional vector Δd, which can be used as a "measure" of the transition. Then we calculated the normalized displacements of the atoms in the average structure obtained in the MD simulation for a certain temperature from their ideal positions in the *Pnam* structure and used these displacements to construct a $3N$-dimensional vector $\Delta d'$. Then the inner product of these two vectors gave the order parameter Q, i.e., $Q = \Delta d \cdot \Delta d'$, which indicates the percentage completeness of the phase transition.

This order parameter is plotted in Fig. 6. As can be seen, at temperatures as high as 600 K, the order parameter already deviates quite substantially from the value of zero, the value for a perfect *Pnam* structure. This results, as we pointed out before, from the average time at these temperatures in our MD simulation not being long enough to average out the disordering of the structure. However, Q fluctuates between positive and negative values above 300 K, as a result of the fact that many
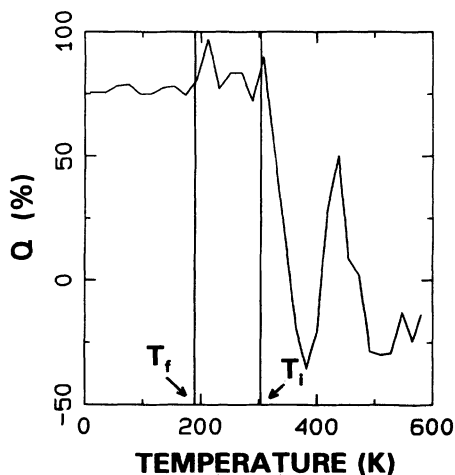
ZnCl$_4$$^{2-}$ ions are still hopping between their two possible disordered orientations. This shows that the structure at these temperatures are still in the *Pnam* phase.

At about 300 K, Q suddenly jumps to a large value and its sign fluctuations disappear. This indicates that the molecular ions are no longer able to switch between the two possible disordered orientations and thus a phase transition has taken place. The theoretical transition temperature is thus at about 300 K, in good agreement with the experimental value of 303 K for the incommensurate phase transition.

It is seen in Fig. 6 that, at temperatures immediately below 300 K, the order parameter still shows noticeable fluctuations. This could be because the system is trying to become incommensurate in conflict with the periodic boundary condition forced unto it. Around 180 K these fluctuations suddenly become much smaller, indicating that the lock-in transition has taken place. This is in general agreement with the experimental transition temperature of 189 K. (The reason why the order parameter Q does not approach 100%, the value for Q if the structure is exactly the theoretical *Pna*2_1 structure, is as follows: at relatively high temperatures there are still substantial amounts of thermal motions that cannot be averaged out due to the limited average time in the MD simulation; while at lower temperatures, the periodicity of the system changes along the *b*- and *c*-axis directions, as will be discussed below, so that the structure will never reach the theoretical *Pna*2_1 structure.)

As the temperature decreases further, the thermal fluctuations of the atoms become much smaller and the average structure begins to show a clear periodicity change. Specifically, it doubles along both the **b** and **c** axes, in addition to the tripling along the **a** axis, which results from the earlier phase transition. At the same time the original orthorhombic lattice becomes monoclinic, i.e., the angle between the **a** and **c** axes deviates from 90°, while the other two lattice angles remain at 90°. At 10 K the monoclinic angle is 90.45°. In Fig. 7 we give the projec-

FIG. 6. The order parameter Q as a function of temperature. T_i and T_f equal the experimental incommensurate transition temperature (303 K) and the ferroelectric lock-in transition temperature (189 K), respectively.
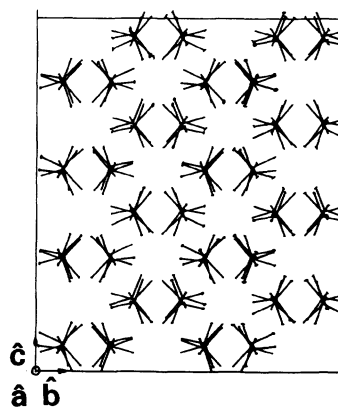

FIG. 7. Projections of the average atomic positions (with the Rb atoms omitted) along the a axis at 10 K obtained from the molecular-dynamics simulation described in the text. The very small thermal ellipsoids are centered at the average atomic positions. The Zn—Cl bonds (straight lines) show the modulation pattern of the structure.

tions of the atomic positions and thermal ellipsoids on the **bc** plane in the average structure at 10 K; for clarity the Rb ions have been omitted.

In Fig. 7, the orientations of the Zn—Cl bonds clearly show that the original twofold periodicity along the **b** axis and fourfold periodicity along the **c** axis in the super-cell have disappeared and the structure is doubled along both **b** and **c** axes. A convenient way to express numerically this change of periodicity is to calculate the root-mean-square difference R between the atomic positions in the average structures and their positions in an ideal structure that retains one of the original periods in the supercell. Obviously, R would be zero if no periodicity changes. In Fig. 8, we plot the values of R as a function of temperature for the twofold period along the **b** axis (∇), fourfold period along the **c** axis ($\square$) and the twofold period along the **c** axis ($\triangle$). At higher temperatures, all three curves have nonzero values. This again results from the fact the random thermal motions of the atoms were not fully averaged out in our MD simulation. Therefore, as the temperature decreases, the values of R decrease as well. But near and below 100 K, the curves for both the twofold period along the **b** axis and the four-fold period along the **c** axis rise rapidly, indicating the breakdown of these periodicities within the supercell. But, at the same time, the curve for the twofold period along the **c** axis still exists, although the size of the super-cell allows the breakdown of this periodicity. Therefore, the lower temperature structure we have reached by MD simulation is doubled along both the **b** and **c** axes, and thus has 48 formula units per unit cell. The theoretical transition temperature is ≤ 100 K, in general agreement with the experimental value 74 K.[19]

Although it has been established that the lower-temperature phase of Rb_2ZnCl_4 has a monoclinic lattice, no experimental determination of the atomic po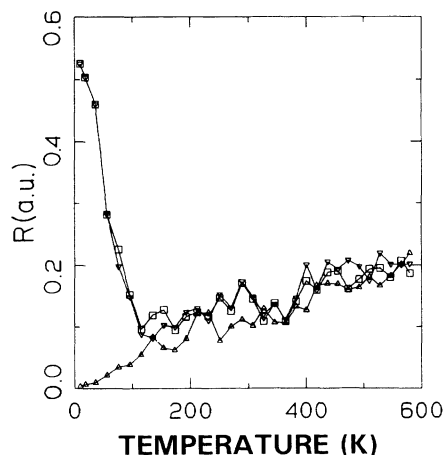sitions has been reported and different suggestions have been made for the specific space-group symmetry. Starting from certain symmetry considerations, Dvorak and Kind[20] found three possible space-group symmetries $Pc11$, $B11a$, and $P1$. Wada et al.[9] also performed Raman measurement and concluded that the lower-temperature cell is double that of the $Pna2_1$ structure, and thus suggested $P2_111$ as its space-group symmetry. Later, Volkov et al.[21] performed submillimeter spectroscopy studies of the acoustic phonons in Rb_2ZnCl_4, and suggested that the space group is likely to be $A11a$ ($=B11a$) rather than $Pc11$ or $P1$.

Recently, Mashiyama[22] reported a single-crystal x-ray study of K_2CoCl_4, another member of the A_2BX_4 family, that has the same phase sequence and is isomorphous to Rb_2ZnCl_4 in all three high-temperature phases, i.e., the $Pnam$, the incommensurate, and the $Pna2_1$. It was determined that the lower-temperature structure of this compound has the space group symmetry $C1c1$ ($=A11a$). The unit cell contains 48 formula units per cell, which is a result of doubling the $Pna2_1$ unit cell along the **b** and **c** directions, respectively. This is consistent with our present result for Rb_2ZnCl_4 from the MD simulation, indicating that the lower-temperature structure of Rb_2ZnCl_4 should be $C1c1$. As will be shown in the next section via lattice-dynamics calculations, the $Pna2_1$ structure is unstable at the point $\mathbf{q}=\mathbf{b}^*/2+\mathbf{c}^*/2$ in the Brillouin zone. This instability will double the $Pna2_1$ unit cell along both the **b** and **c** axes, which is precisely the result of our MD simulation.

However, when we compared the actual atomic positions in our simulated structure from the lower-temperature phase of Rb_2ZnCl_4 with those reported for K_2CoCl_4,[22] we found that the patterns of modulations that cause the doubling along the **b** and **c** directions in the two structures are different. Moreover, the monoclinic lattice angle 90.45° in the theoretical structure (Fig. 7) is too large compared with the value 90.03° for K_2CoCl_4. Thus, we question whether our theoretical structure for the low-temperature phase is exactly the correct structure, or just one of the many that are energetically close to the correct structure but accessible only in the simulation. For a MD simulation with fairly large and complex supercell, it would not be surprising that the system locks into such a point in the phase space as a result of the statistical uncertainties inherent in MD simulations with limited sample size and time.

Since the $Pna2_1$ structure contains the instability that doubles the structure, as mentioned above, an alternative way to reach the doubled structure is to lift the $Pna2_1$ symmetry constraints and perform a fast MD relaxation, i.e., to reduce very rapidly the kinetic energy generated by the relaxation. Thus, we started from the theoretical static $Pna2_1$ structure doubled along the **b** axis and quadrupled along the **c** axis to allow the anticipated structural changes and relaxed it very quickly. Then the sample was maintained at 10 K for 20 ps, while the average positions of the atoms were calculated. The **bc**-plane cross section of the obtained average structure is shown in Fig. 9, again with Rb atoms omitted for clarity. The modulation patterns in Fig. 9 are now exactly the same as those
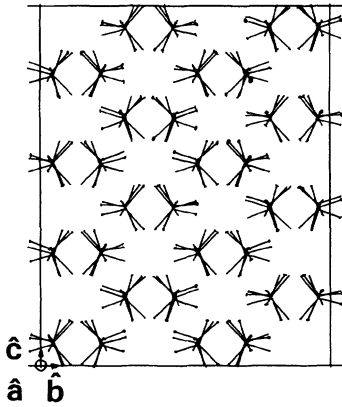

FIG. 8. Supercell periodicity parameter R as a function of temperature for the twofold period along the b axis (∇), four-fold period along the c axis ($\square$), and twofold period along the c axis ($\triangle$).

FIG. 9. Average atomic positions (projection along the *a* axis) in the MD average structure at 10 K. The Rb atoms have been omitted. The modulation pattern shown by the Zn—Cl bonds (straight lines connecting each Zn and the four nearest Cl atoms) is very similar to that found for K_2CoCl_4 (Ref. 22).

FIG. 10. Dispersion curves along the [100] direction for the theoretical *Pnam* structure.

found for K_2CoCl_4. The monoclinic angle, i.e., the angle between the **a** and **c** axes, is now 90.06°, which is much closer to the experimental value 90.03° for K_2CoCl_4.[22]

While this new structure is more likely to be the real structure, its average potential energy is, however, slightly higher than the earlier structure (Fig. 7) by 0.28 meV per formula unit. This difference is negligible when compared with the energy difference of 61 meV per formula unit between the average potential energy for the $Pna2_1$ structure at 75 K and that for the structure in Fig. 7. This means that, at the $Pna2_1$-monoclinic phase transition, the preference for the structure in Fig. 7 is dominated by the entropy contribution to the free energy. When the temperature is further lowered so that the small energy difference becomes important, there might be a high activation barriers between the structure in Fig. 9 and that in Fig. 7. These suggestions are, of course, subject to proof by MD simulations with even larger samples and longer times, which are definitely beyond our computing resources. But it is clear from the present study that the lower-temperature phase of Rb_2ZnCl_4 has the space-group symmetry of $C1c1$ and has 48 formula units per cell.

V. LATTICE-DYNAMICS CALCULATIONS

In our previous study of K_2SeO_4, a lattice-dynamics calculation using the *ab initio* interionic potentials successfully revealed the lattice instability in the *Pnam* structure with the theoretical wave vector of the instability in excellent agreement with experiment.[8] A zone-center instability was also found and was shown to reflect the double-well structure on the potential energy surface, which is ultimately responsible for the phase transitions in K_2SeO_4. Since Rb_2ZnCl_4 is isomorphous with K_2SeO_4 for all the *Pnam*, incommensurate, and the $Pna2_1$ phases, we expect similar results from the lattice-dynamics calculations.

In Fig. 10, we plotted the angular frequency squared (ω^2) divided by $|\omega|$ vs wave vector q for the lowest ten
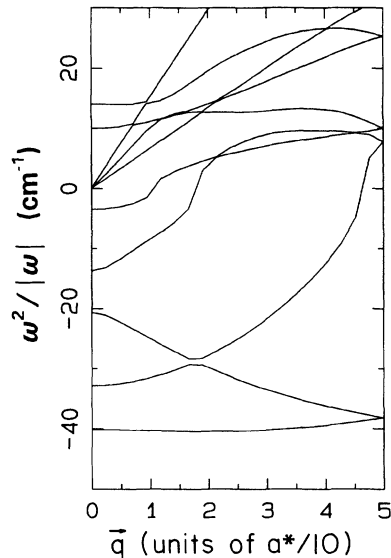
branches of the dispersion curves for the [100] (Σ) direction of the theoretical *Pnam* structure obtained in Sec. III (negative values represent imaginary frequencies). Figure 10 contains several negative branches, indicating that the *Pnam* structure is actually unstable. This is similar to the situation for K_2SeO_4 and is consistent with experiment, since the *Pnam* structure does transform at lower temperatures. However, the most negative point on the dispersion curves, representing the dominant instability, occurs at about $q=0.18a^*$ rather than near $q=a^*/3$, which would be more consistent with the observed incommensurate and the lock-in cell-tripling transitions. This is very different from the case of K_2SeO_4 where the theoretical maximum instability occurs at $q=0.304a^*$, which is very close to the experimental soft-phonon wave vector $q=0.31a^*$.

This discrepancy is not surprising if we recall that, although the *Pnam* structures for both Rb_2ZnCl_4 and K_2SeO_4 just above the incommensurate phase transition are disordered, the disordering in the former is much more "severe" than in the latter, as we discussed in the previous section. Therefore, while a dispersion calculation for a perfect *Pnam* structure is still more or less relevant for K_2SeO_4, it is less so to Rb_2ZnCl_4 in the temperature range near the incommensurate transition, which may explain the above "mismatch" of the wave vectors.

The difference in "severity" of the disordering in the *Pnam* structures of the two crystals could be the reason which experimentally K_2SeO_4 exhibits a well-defined soft-phonon behavior for the incommensurate phase transition while Rb_2ZnCl_4 does not.[1] In K_2SeO_4 the transition is from a "slightly" disordered *Pnam* phase to the incommensurate phase, while in Rb_2ZnCl_4 the transition may be viewed as two steps: first from a "slightly" disordered *Pnam* structure at high temperatures to a "highly" disordered *Pnam* structure at lower temperatures, al-

though the disordering is purely dynamic, and then to the incommensurate structure. Therefore, the actual transition is more of an order-disorder type; hence, the absence of the soft-phonon behavior associated with purely displacive phase transitions. Hence, our dispersion curves in Fig. 10 can, at most, be used to describe a "slightly" disordered Pnam structure of Rb_2ZnCl_4 which perhaps exists at a much higher temperature than the incommensurate transition temperature where the time scales of the disordering would become compatible with those in K_2SeO_4, due to the increase of kinetic energy. Nevertheless, they illustrate the basic structural instabilities in the system. As in the case of K_2SeO_4, the negative branches of dispersion curves in Fig. 10 extend over the whole zone, indicating the multiple instabilities. The most interesting of these is at the zone center, involving a structural change within the unit cell. To probe this change we performed molecular-dynamics relaxations to $T = 0$ K for a single Pnam unit cell of Rb_2ZnCl_4 without any constraints besides the periodic boundary conditions. We found two additional, stable singlet structures that have exactly the same static energy but appear as mirror images of each other. The projections of the atomic positions along the a axis for these two structures are plotted in Fig. 11. If we compare Fig. 11 with the theoretical Pnam structure in Fig. 2(a), we see that these structures are formed by rotations of the $ZnCl_4^{2-}$ ions and shifting of the Rb^+ ions with equal amplitudes but in opposite directions. This is exactly the same as the result in our previous study of K_2SeO_4: the potential-energy surface for a single Pnam unit cell has a double-well structure with the Pnam structure at the top and the structures in Fig. 11, at the bottoms of the two wells. When the
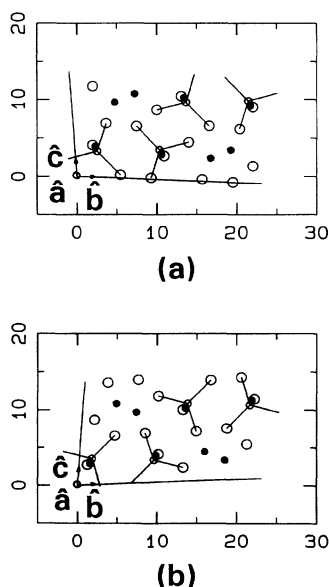
periodicity along the a axis is changed, this double well generates a multiple-well structure on the total potential-energy surface, which is the origin of the $Pnam$-$Pna2_1$ cell-tripling transition.

The energy difference between the static Pnam structure in Fig. 2 and that of the singlet structures in Fig. 11 is 109.8 meV per formula unit, much larger than the corresponding value of 12.3 meV for K_2SeO_4; hence, the double well in Rb_2ZnCl_4 is much deeper. This explains why the Pnam phase of Rb_2ZnCl_4 at room temperature is so much more disordered than K_2SeO_4. Another factor is the much larger masses of the Cl atoms compared with the O atoms, which produce a much slower time scale for the librations of the $ZnCl_4^{2-}$ ions.

The energy for the static $Pna2_1$ structure in Fig. 4 is 94.1 meV per formula unit lower than that for the Pnam structure in Fig. 2, while the static energy for the monoclinic structure in Fig. 7 is 1.1 meV lower than the $Pna2_1$ structure. The sequence of these energy levels agree with the order in which these structures appear in our molecular-dynamics "quenching." Both the $Pna2_1$ and monoclinic structures have static energies higher than that for the singlet structures in Fig. 10, by 15.7 meV for the former and 14.6 meV for the latter. However, our molecular-dynamics "quenching" did not find either of these singlet structures but rather first selected the tripled $Pna2_1$ structure and subsequently the monoclinic structure that multiplied the Pnam unit cell 12 times. This is not surprising if we notice that the 15.7-meV difference between the $Pna2_1$ and the singlet structures is relatively small compared with the 94.1-meV difference between the $Pna2_1$ and the Pnam structures. At the time of the transition, the tripled $Pna2_1$ structure is more favorable than the singlet structure, since the former has a higher entropy due to the fact that the $ZnCl_4^{2-}$ ions have three rather than one possible orientations. Subsequently, for the $Pna2_1$ structure to transform to the singlet structure in Fig. 11, it requires that at least one of the tetrahedra switch through the Pnam configuration. When the temperature is below the $Pnam$-$Pna2_1$ transition, this transformation is frustrated by the ~94.1-meV activation barrier and the $Pna2_1$ persists until the $Pna2_1$-monoclinic transition which does not involve such switching of the $ZnCl_4^{2-}$ ions.

Next we examine the lattice-dynamics properties of the $Pna2_1$ structure, which is perfectly ordered. In Fig. 12 we plot a few of the lowest dispersion curves along the [011] direction. As can be seen, four branches become negative and reach their maximum negative value at the point $q = b^*/2 + c^*/2$ where they become doubly degenerate. This shows that the $Pna2_1$ structure has a doubling instability along both the b and c axis, exactly as we found from our molecular-dynamics calculations discussed in the previous section. (For comparison, we have also calculated the same dispersion curves for the $Pna2_1$ structure of K_2SeO_4 and found no negative values at any part of the Brillouin zone. This is also consistent with the result from our MD simulation[8] that K_2SeO_4 does not undergo a similar transformation. There has been no experimental report of such a transformation in K_2SeO_4.)

(a)

(b)

FIG. 11. The bc-plane cross sections of the two energetically equivalent singlet structures of Rb_2ZnCl_4 obtained from single-cell (Pnam) molecular-dynamics relaxations. The lengths of the lattice axes are given in atomic units.
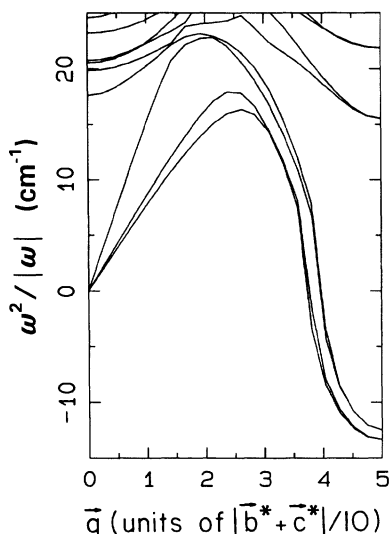
FIG. 12. Dispersion curves along the [011] direction for the theoretical $Pna2_1$ structure.

In a study of the $Pna2_1$-monoclinic phase transition of Rb_2ZnCl_4 by Raman scattering, Wada et al. found a doubly degenerate mode which shows in Raman spectra only at temperatures below the transition and softens as the transition temperature is approached. Since all of the zone-center modes in the $Pna2_1$ symmetry are Raman active, they concluded that this mode must be at the Brillouin zone boundary of the $Pna2_1$ phase. Further, they put forward the conjecture that the lower temperature phase must double the $Pna2_1$ structure along one of the lattice axes and thus has 24 formula units per cell.

Now we see that our present theoretical results provides another explanation to the experimental data of Wada et al.[9] these modes are not at the boundary but the corner of the Brillouin zone and the lower-temperature phase doubles the $Pna2_1$ structure not along just one direction, but along both the b and c directions.

Rb₂ZnCl₄ and performed static relaxations, molecular-dynamics simulations, and lattice-dynamics calculations. The theoretical static structures for both the Pnam and the $Pna2_1$ phases were found to be in close agreement with experiment. The molecular-dynamics calculations successfully simulated the phase transitions from the Pnam phase to the $Pna2_1$ phase with the transition temperature close to the experimental value. For the lower-temperature, monoclinic phase, whose detailed structure is not yet known experimentally, our results for both MD simulation and lattice-dynamics calculation show that it should be double the $Pna2_1$ structure along both the b and c axes, thus giving a unit cell containing 48 formula units. Also, by lattice-dynamics calculations and molecular-dynamics relaxations, we have shown that the potential-energy surface pertinent to the phase transitions contains a double-well structure, very similar to that of K_2SeO_4. However, the double wells in Rb_2ZnCl_4 are much deeper in energy, giving rise to a much more disordered Pnam phase above the incommensurate transition, which is probably the reason why the incommensurate phase transition in K_2SeO_4 displays a soft-phonon character while the same transition in Rb_2ZnCl_4 does not.

Compared with the previous polarizable-ion model[4] for Rb_2ZnCl_4, our present method gives equally good agreement with experiment, if not better; moreover, the comparison between theory and experiment made here is much more extensive than in Ref. 4. We believe that, for ionic molecular crystals, the present approach is more suitable. This is because the main difference between these crystals and the purely ionic systems well described by the fully ionic rigid-ion model is the electron covalency within the molecular ion which causes a charge transfer between the constituent atoms within the ion. The present approach is also more fundamental in nature, since all of the potentials are generated ab initio, unlike the polarizable-ion model where an artificial polarization function has to be postulated, and is computationally advantageous, since it involves fewer degrees of freedom and can therefore be used to treat larger systems.

VI. CONCLUSION

We have applied our recent method for generating ab initio interionic potentials for ionic molecular solids to

ACKNOWLEDGMENT

[1]An extensive review can be found in H. Z. Cummins, Phys. Rep. **185**, 211 (1990).

[2]V. Katkanant, P. J. Edwardson, J. R. Hardy, and L. L. Boyer, Phys. Rev. Lett. **57**, 2033 (1986).

[3]P. J. Edwardson, V. Katkanant, J. R. Hardy, and L. L. Boyer, Phys. Rev. B **35**, 8470 (1987).

[4]P. J. Edwardson and J. R. Hardy, Phys. Rev. B **38**, 2250 (1988).

[5]V. Katkanant, P. J. Edwardson, J. R. Hardy, and L. L. Boyer, Phase Transitions **15**, 103 (1989).

[6]R. G. Gordon and Y. S. Kim, J. Chem. Phys. **56**, 3122 (1972).

[7]M. Quilichini and J. Pannatier, Acta Crystallogr. B **39**, 657 (1983).

[8]H. M. Lu and J. R. Hardy, Phys. Rev. Lett. **64**, 661 (1990); Phys. Rev. B **42**, 8339 (1990).

[9]M. Wada, A. Sawada, and Y. Ishibashi, J. Phys. Soc. Jpn. **50**, 531 (1981).

[10]V. Day (private communication).

[11]E. Clementi and C. Roetti, At. Data Nucl. Data Tables **14**, 177 (1974).

[12]R. S. Mulliken, J. Chem. Phys. **23**, 1833 (1955).

[13]M. J. Frisch et al., GAUSSIAN 86 (Carnegie-Mellon Quantum Chemistry Publishing Unit, Pittsburgh, PA, 1984).

[14]K. Itoh, A. Hinisada, H. Matsunaga, and E. Nakamura, J. Phys. Soc. Jpn. **52**, 664 (1983).

[15]K. Itoh, A. Hinasada, M. Daiki, and E. Nakamura, J. Phys. Soc. Jpn. **58**, 2070 (1989).

[16]Sawada, Y. Shiroishi, A. Yamamoto, M. Takashige, and M. Matsuo, J. Phys. Soc. Jpn. **43**, 2099 (1977).

[17]M. Parrinello and A. Rahman, Phys. Rev. Lett. **45**, 1196 (1980).

[18]V. Katkanant, J. R. Hardy, and F. G. Ullman, Ferroelectrics **82**, 185 (1988).

[19]P. Gunter, R. Sanctuary, F. Rohner, H. Arend, and W. Seidenbusch, Solid State Commun. **37**, 883 (1981).

[20]V. Dvorak and R. Kind, Phys. Status Solidi B **107**, K109 (1981).

[21]A. A. Volkov, Yu. G. Goncharov, G. V. Kozlov, V. I. Torgashev, J. Petzelt, and V. Dvorak, Ferroelectrics **109**, 363 (1990).

[22]H. Mashiyama, J. Phys. Soc. Jpn. **60**, 180 (1991).